Supplement of Earth Syst. Sci. Data, 16, 1875–1900, 2024
https://doi.org/10.5194/essd-16-1875-2024-supplement

Open Access Earth System Science Data

Supplement of

High-resolution physicochemical dataset of atmospheric aerosols over the Tibetan Plateau and its surroundings

Jianzhong Xu et al.

Correspondence to: Jianzhong Xu (jzxu78@sjtu.edu.cn, jzxu@lzb.ac.cn) and Xinghua Zhang (zhangxinghua@lzb.ac.cn)

S1. HR-ToF-AMS operation

The HR-ToF-AMS is one of the most advanced instruments that widely used for the study of atmospheric aerosol chemistry worldwide. The detailed principle of HR-ToF-AMS can be obtained elsewhere (DeCarlo et al., 2006). The HR-ToF-AMS is mainly composed by three different sections that separated by small apertures and differentially pumped, i.e., a particle beam generation section to form a concentrated and narrow particle beam through a critical orifice and a six-stage aerodynamic lens, a particle-sizing chamber to measure the particle aerodynamic sizes through a particle time-of-flight measurement (different velocities and arrival times for size-dependent particles in a known flight distance), and a particle chemical composition detection section to directly vaporize the particle beam at a ~600 ℃ resistively heated surface, ionize the particles into positively charged ion fragments by a 70 eV electron impact, and then detect their chemical composition by a high-resolution mass spectrometer (Jimenez et al., 2003).

There are two different operation modes in HR-ToF-AMS, i.e., V-mode (detection limits of about 10 ng m^{-3}) and W-mode (~5000 m/Δm) with different signal-to-noise ratio (S/N). However, the HR-ToF-AMSs were only operated at the V-mode during almost all the seven field campaigns in consideration of the relatively low aerosol mass concentration level and low S/N ratio over the TP. The mass concentration and size distribution of non-refractory PM_1 chemical species were obtained by further switching the instrument between mass spectrum (MS) mode and particle time-of-flight (PToF) mode every 15s under the V-mode operation. However, there are no observation of particle sizes during the NamCo and LHG measurements due to the malfunction of the chopper. In addition, the HR-ToF-AMS need to be calibrated for its flow, ionization efficiency (IE), and sizes at the beginning and end of each observation (Jayne et al., 2000). The relative IE (RIE) of ammonium and sulfate were calibrated using the mono-dispersed pure ammonium nitrate and ammonium sulfate particles, respectively, with the selected sizes of 200–300 nm, while the particle size was calibrated using the mono-dispersed ammonium nitrate particles with sizes varied from 60 to 600 nm. Finally,

default RIE values were assumed to be 1.1, 1.3, and 1.4 for nitrate, chloride, and OA, respectively, during all the field campaigns, while different RIE values were set for ammonium and sulfate according to their calibration results during each campaign, e.g., 3.9 and 4.2 for ammonium and 1.6 and 1.4 for sulfate based on two calibrations in the QOMS measurement.

S2. HR-ToF-AMS data processing

The HR-ToF-AMS data was processed using the standard data analysis software with SQUIRREL and PIKA toolkits written in Igor Pro (Wavemetrics Inc., Lake Oswego, OR, USA). The SQUIRREL used a fragmentation table to apportion the measured signals at each mass-to-charge ratio (m/z) into different species to quantify the chemical composition of non-refractory PM_1 species, while the PIKA employed a modified Gaussian fitting algorithm to obtain the ion-speciated high-resolution mass spectra (HRMS) and elemental composition of OA (Allan et al., 2004; DeCarlo et al., 2006). The elemental ratios of OA, i.e., oxygen-to-carbon (O/C), hydrogen-to-carbon (H/C), organic matter-to-organic carbon (OM/OC), and nitrogen-to-carbon (N/C), were determined using the improved method (Canagaratna et al., 2015) during all the seven observation campaigns.

In addition, a collection efficiency (CE) was generally introduced to compensate for the incomplete transmission and detection of particles through the aerodynamic lens and bouncing at the vaporizer surface in most AMS studies. Previous study has revealed that the CE is significantly influenced by the relative humidity (RH) in sampling line and the acidity and ammonium nitrate mass fraction (ANMF) in the sampled aerosols, which has been concluded as a build-in composition-dependent CE (CDCE) algorithm in the standard data processing software (Middlebrook et al., 2012). Generally, a high RH, a high aerosol acidity, or a high ANMF often corresponds to a high CE value. However, the RH in the sampling system is always maintained below 40% due to the professional deployments of dryers in the front of the sampling system and the ANMF is basically below 0.4 due to the low contributions of nitrate and ammonium during all the seven observation campaigns, which means the negligible effects of these two

parameters on CE in our study. Therefore, default CE value of 0.5 were finally employed during the QOMS, NamCo, Ngari, Waliguan, and Lhasa campaigns in consideration of their overall neutralized or slightly acidic aerosols, whereas the CDCE values were adopted at Motuo, LHG, and Bayanbulak where bulk submicron aerosols were acidic.

S3. OA source apportionment using PMF analysis

Source apportionment of OA during each observation was conducted by the positive matrix factorization (PMF) analysis on organic matrix data using the PMF2.exe algorithm in robust mode (Paatero and Tapper, 1994) and the standard PMF Evaluation Tool (PET, Ulbrich et al., 2009) written in Igor Pro software.

The PMF analysis was evaluated thoroughly according to the standard procedures outlined in Zhang et al. (2011) by down-weighting, modifying, or removing some ion fragments in the data and error matrices. Firstly, those ions at m/z >120 and all the isotope ions were generally excluded because of the insufficient ability to resolve the deconvolution due to their low signals. Then, the signals of the four organic ions of O^+, HO^+, H_2O^+, and CO^+ were scaled to that of CO_2^+ according to the suggested fragmentation table in Aiken et al. (2008) and further down-weighted in PMF analysis. Thirdly, all those "bad" ions (S/N <0.2) were removed from the data matrices, while all the "weak" ions (0.2< S/N <2) were downweighted by increasing their errors. In addition, some runs and some ions which had obviously huge residual spikes were also removed in order to avoid their unnecessary interference. After the above pre-processing, the PMF solutions were investigated by selecting a certain variation range of factor number and rotational parameter (*f*Peak), e.g., 1−6 factors with *f*Peak varying from –1 to 1. Finally, the optimal solution of PMF analysis were determined after a comprehensive evaluation by examining the model residuals at each m/z and each time, comparing the factor mass spectrum with corresponding reference spectrum, comparing the temporal variation of individual factor with external tracers, and analyzing the diurnal variation pattern of each factor. Totally, 2-, 3-, or 4-factor solution were selected during the different field campaigns in this study. The specific high-resolution mass

spectrum of each OA factor identified among the eight different field campaigns are shown in Figure S4.

S4. Operation and data processing of other instruments

1) SMPS

The scanning mobility particle sizer (SMPS) developed by the TSI Inc. is composed by an electrostatic classifier (EC, model 3080) equipped with a long-differential mobility analyzer (long-DMA, model 3081) and a condensed particle counter (CPC, model 3772). Ambient particles are first screened by a particle impactor installed at the front of the DMA and large particles are removed. Ambient particles are measured through an electrical mobility detection technique in this instrument, e.g., a bipolar charger in the EC is utilized to charge the particles to a known charge distribution, then classify them according to their ability to traverse an electrical field in the long-DMA, and finally count those screened monodisperse particles by the CPC. The sample and sheath flow rates are 0.3 and 3.0 L min^{-1}, respectively, at both QOMS and Lhasa which measure particles between 14.6 and 661.2 nm in mobility diameter (D_m), whereas the sample and sheath flow rates are 0.5 and 5.0 L min^{-1} at LHG and Motuo and sample particles at a size range of 10.9−495.8 nm in D_m. The number concentrations of submicron particles in 107 different size channels are firstly recorded at an initial time resolution of 5 min and then converted to the total number and volume concentrations according to the obtained size distribution of number concentration.

2) PAX

The PAX directly measures the B_{abs} and B_{scat} of aerosol particles at 405 nm by using a modulated diode laser, namely measures the B_{abs} by an in-situ photoacoustic technique while the B_{scat} using a wide-angle integrating reciprocal nephelometer. The B_{ext} is the sum of B_{abs} and B_{scat} while the single scattering albedo (SSA) is calculated as the ratio of B_{scat} to B_{ext}. The BC mass concentration is calculated as the ratio of measured B_{abs} to a fixed BC mass absorption cross-section (MAC) value of 10.19 m^2g^{-1} at 405 nm. In addition, the B_{scat} is calibrated using the high-concentration ammonium sulfate particles generated by the aerosol generator, while the B_{abs} is calibrated using the

sufficient black smoke from a kerosene lamp before each field campaign according to the operator manual of this instrument.

3) Aethalometer

The Aethalometer (models AE31 or AE33) is used to measure the particle B_{abs} at seven wavelengths, which firstly measures the light attenuation between particle-laden and particle-free sample spots on the filter and finally converts the attenuation to particle B_{abs} in ambient air. Both AE31 and AE33 have seven bands, namely 370, 470, 520, 590, 660, 880 and 950 nm, and the concentration of black carbon is mainly measured according to the absorption coefficient at 880 nm. The filter-based loading effect and multiple scattering effect are corrected during all the three observations to eliminate the difference between the light attenuation measured at the filter and the ambient particle B_{abs}.

The absorption Ångström exponents (AAE) value is acquired through a power-law fitting of B_{abs} following the typical Beer-Lambert's law, i.e., $AAE = ln(B_{abs,\lambda1}/B_{abs,\lambda2})/ln(\lambda_2/\lambda_1)$. Furthermore, a traditional AAE method was adopted to quantitatively apportion the total B_{abs} into two parts from BC and BrC ($B_{abs,BC}$ and $B_{abs,BrC}$) at 370−660 nm during each campaign. The contribution of BrC to total B_{abs} ($fB_{abs,BrC}$) at a short wavelength λ is calculated as $fB_{abs,BrC,\lambda} = 1 - (B_{abs,880}/B_{abs,\lambda}) \times (\lambda/880)^{-AAE_{BC}}$ by assuming its negligible contribution at 880 nm. Detailed information about the data correction and calculation of this instrument can be found in our previous publication (Zhang et al., 2021b).

4) CCN-100

The CCN-100 measures aerosol particles called cloud condensation nuclei that can form into cloud droplets. The instrument supersaturates the sampled aerosol particles in a 50-cm-high column with continuously wetted walls and a longitudinal thermal gradient, so that those particles grow into detectable CCN particles and are measured using an optical particle counter among 20 different size bins. The principle of CCN counters is that diffusion of heat in ambient air is slower than that of water vapor, which diffuses from the warm, moist column walls to the centerline faster than heat in the

column. Detail information may refer to Roberts and Nenes (2005). The number concentrations of CCN are measured consecutively at five different *SS* values of 0.2%, 0.4%, 0.6%, 0.8%, and 1.0%. The CCN data is recorded every 5 minutes at each *SS* and finally has a time resolution of 30 minutes during a complete measurement cycle.

S5. Calculation and evaluation of the bulk acidity of submicron aerosols

Bulk acidity of submicron aerosols from AMS measurement was generally evaluated following the methods in Zhang et al. (2007) and Schueneman et al. (2021). The mass concentration of ammonium was firstly predicted by assuming to fully neutralize these AMS measured sulfate, nitrate, and chloride using the following equation (S1):

$$NH_{4\ Predicted}^{+} = 18 \times (2\times SO_4^{2-}/96 + NO_3^{-}/62 + Cl^{-}/35.5) \quad (S1)$$

Then, the mass concentration ratio of measured ammonium to predicted ammonium ($NH_{4\ Measured}^{+}/NH_{4\ Predicted}^{+}$) was further calculated to be a good indicator to evaluate the bulk acidity of submicron aerosols. In this study, linear regression analysis between the mass concentrations of measured and predicted ammonium was performed to evaluate the bulk acidity of submicron aerosols in the different TP regions (Fig. 3). Aerosol particles are generally considered to be "acidic" if the calculated ratio is obviously lower than 1 and to be "more acidic" if the ratio is lower than 0.75, whereas a ratio that roughly near to 1 or larger than 1 indicates the particles are "bulk neutralized" and even there are more excess ammonium that needed to be neutralized. Note that the validity of using this method is based on the assumption that the influence from nitrogen- or sulfur-containing organic ions (e.g., organic acids and organic nitrogen compounds) as well as the mineral and metal ions are negligible (Zhang et al., 2007).

S6. Estimation of aerosol DRFs using the SBDART and OPAC models.

The aerosol direct radiative forcing (DRF) was modelled by the widely used Santa Barbara DISORT (Discrete Ordinate Radiative Transfer) Atmospheric Radiative Transfer (SBDART) model in the shortwave spectral range of 0.25−4.0 μm. SBDART is a software tool that computes the plane-parallel radiative transfer under both clear

and cloudy conditions (Ricchiazzi et al., 1998). Specific simulation of aerosol DRF in the atmosphere (ATM) can be described by the following equations (2) and (3). In brief, the net fluxes (ΔF, difference between the downward and upward radiation fluxes) with and without the investigated variable were calculated twice in this model under cloud-free conditions at both the earth's surface (SUR) and the top of the atmosphere (TOA). The differences of net fluxes between the two simulations were then considered as the DRFs of the specific investigated variable at the SUR and TOA. Finally, the DRF in the ATM (DRF^{ATM}) was obtained using the DRF at TOA (DRF^{TOA}) minus the DRF at SUR (DRF^{SUR}). The details of the model description can be found in previous studies (Xin et al., 2016; Gong et al., 2017).

$$\Delta F = F^{\text{downward}} - F^{\text{upward}} \quad \text{(S2)}$$

$$\text{DRF}^{\text{ATM}} = \text{DRF}^{\text{TOA}} - \text{DRF}^{\text{SUR}} = (\Delta F^{\text{TOA}}_{\text{with}} - \Delta F^{\text{TOA}}_{\text{without}}) - (\Delta F^{\text{SUR}}_{\text{with}} - \Delta F^{\text{SUR}}_{\text{without}}) \quad \text{(S3)}$$

The principle and specific steps for the estimation of aerosol DRFs using the SBDART mode can be described briefly as follows:

Firstly, the mass concentrations of organic carbon (OC), BC, and water-soluble ions (WSIs), which were measured from the corresponding off-line filter samples with one- or two-days time resolutions during each campaign, were the initial measured parameters used for the estimation of aerosol DRFs.

Then, the particle numbers of each species in per cubic meter air (denoted as ρ_n) were estimated using the above measured mass concentrations of each species divided by the referred M values in the OPAC model (Hess et al., 1998), which represented the aerosol mass in per cubic meter air and integrated over the size distribution and normalized to 1 particle per cubic centimeter of air. Specifically, values of 5.99E-5 was used for soot/BC particles and 1.34E-3 were used for OC and WSIs.

Next, four crucial input optical parameters of aerosol optical depth (AOD), single scattering albedo (SSA), Ångström exponent (AE), and asymmetry factor (ASY), and the light absorption and scattering coefficients were estimated for OC, BC, WSIs and total particles, respectively, using the Optical Properties of Aerosol and Cloud (OPAC)

model. Detailed introduction of OPAC model can be found in Hess et al. (1998). Noting that the above estimation in OPAC model were performed six times during each campaign by setting the ρ_n as the above calculated value multiplier 1 to 6, respectively.

Then, the entire six datasets of modelled total light absorption and scattering coefficients were further used to evaluate the performance of OPAC model by comparing them with those corresponding measured light absorption and scattering coefficients from PAX and Aethalometer (Figures S6-10). Finally, the optimal ρ_n value was selected when the modelled total light absorption and scattering coefficients were comparable.

The performance of the OPAC model was then evaluated and tuned by comparing the modelled total light scattering and absorption coefficients with those correspondingly measured values from online Aethalometer and PAX measurements during the three campaigns, as shown in Figures S5-10. The consistent variation trends were found between them with the coefficient of determination (R^2) varying between 0.69 and 0.99. The slightly lower modelled values compared with those measured values was mainly attributed to their inconsistent wavelengths, i.e., the modelled light scattering and absorption coefficient at 550 nm in the OPAC model, whereas the measured light scattering coefficients at 405 nm for PAX and the light absorption coefficients at 520 nm for Aethalometer. Overall, the small difference between the modelled and measured values indicated the reasonable simulation of aerosol optical parameters (e.g., AOD, AE, SSA, and ASY) in the OPAC model in this study. Finally, these four optical parameters belonging to each species were all used in the SBDART model for the simulation of DRFs caused by OC, BC, and WSIs.

After the above evaluation, the finally obtained four input parameters of AOD, SSA, AE and ASY belong to each species (OC, BC, WSIs, and total particles) were inputted into the SBDART model to simulation the DRFs of each species, respectively.

234 **Table S1. Summary of measurements on ambient aerosols in the TP by different off-line filter sampling and on-line instruments.**

	Measurement content	Period	Site	Instrument/Method	Resolutions	References
	Off-line filter sample analysis for aerosol concentration and chemical composition: CAs (BC/EC/OC/WSOC/BrC), WSIs, element, etc.					
1.	BC and OC dataset over the Third Pole	Different periods during different campaigns	19 stations from APCC network	TSP samples	off-line, 24-48 h	Kang et al. (2022)
2.	CAs characteristics on the Third Pole			TSP samples	off-line, 24-48 h	Chen et al. (2019a)
3.	CAs in the TP: An investigative review		Lhasa, Lulang, Nam Co, QOMS, etc.	$PM_{2.5}$ and TSP samples	off-line	Li et al. (2021a)
4.	BC sources reaching the TP		7 stations across the Himalayas	TSP samples	off-line, 24-48 h	Li et al. (2016a)
5.	Concentrations and light absorption of CAs	2013/5-2014/3	Lhasa, urban city	PM_{10} and $PM_{2.5}$ samples	off-line,12-24h/week	Li et al. (2016b)
6.	CAs (OC and BC)	2006/7-2009/12	Nam Co, inland TP	TSP samples	off-line, 4–14 days	Zhao et al. (2013a)
7.	Mass, elements, CAs, and WSIs	2008/7/16-2009/7/26	Lulang, southeastern TP	TSP samples	off-line, 6 days	Zhao et al. (2013b)
8.	Concentrations, seasonality and sources of CAs	2009/8-2010/7	QOMS, southern TP	TSP samples	off-line, 24 h/week	Cong et al. (2015)
9.	Size distribution of CAs	2012	Nam Co, inland TP	Size-segregated samples	off-line, 72 h	Wan et al. (2015)
10.	Size-segregated characteristics of CAs	2014/8-9,11-12	Lhasa, urban city	Six-stage cascade impactors	off-line	Wei et al. (2019a)
11.	Near surface $PM_{2.5}$ concentration	2016/12/20-12/26	Lhasa, urban city	$PM_{2.5}$ samples	off-line, 12 h	Li et al. (2019)
12.	BC concentrations	2003/12/5-2006/2/17	Muztagh Ata Mountain, northern TP	TSP samples	off-line, 1 week	Zhou et al. (2018)
13.	Elemental concentrations	2005/11-2007/11	Nam Co Station, inland TP	TSP samples	off-line, weekly	Kang et al. (2016)
14.	Elemental composition	2019/12-2020/11	Yaze, southeastern TP	TSP samples	off-line, 15 days	Xu et al. (2022b)
15.	Elements and WSIs	2009/3-5,7-8,11-12	Lijiang, southeastern TP	TSP samples	off-line, 1-2 days	Zhang et al. (2016)
16.	Characteristics of WSIs	2010/7/16-2011/7/28	Qilian Shan, northeastern TP	$PM_{2.5}$ samples	off-line, weekly	Xu et al. (2014)
17.	Seasonal variations and size distributions of WSIs	2012/10-2013/9	Shigatse, southern TP	Eight-stage impactor	off-line, weekly	Yang et al. (2016)
18.	Characteristics of size distributions and sources of WSIs	2014/8-9,11-12	Lhasa, urban city	Six-stage cascade impactors	off-line	Wei et al. (2019b)
19.	OC, EC, WSOC and HULIS	2014/12/21-2015/2/2 2015/8/3-9/7	Nam Co, inland TP	TSP samples	off-line, 12 h	Wu et al. (2018)
20.	Overestimation of BC concentration caused by high OC	2018/7–2019/7; 2020/4–2021/3; 2017/1–2017/12	Yaze, southeastern TP;; QOMS, southern TP; Nam Co, inland TP	TSP samples	off-line, 2-20 days	Hu et al. (2023)
21.	Chemical composition of $PM_{2.5}$ and TSP	2010/6-2010/9	Qinghai Lake, northeastern TP	$PM_{2.5}$ and TSP samples	off-line, 3 days	Zhang et al. (2014)
22.	Chemical characterization and sources of $PM_{2.5}$	2015/5-2016/5	Mt. Gongga, eastern TP	$PM_{2.5}$ samples	off-line, weekly	Meng et al. (2020)
23.	Chemical composition and size distribution of $PM_{2.5}$	2012/7/11-9/6	Qilian Shan, northeastern TP	$PM_{2.5}$ samples	off-line, 3 days	Xu et al. (2015)
24.	Chemical compositions in $PM_{2.1}$	2012/4-2014/12	Mt. Gongga, eastern TP	Nine-stage Anderson sampler	off-line, 48 h	Su et al. (2018)
25.	Chemical composition of size-segregated aerosols	2013/3-2014/2	Lhasa, urban city	Size-segregated samples	off-line, 2 weeks	Wan et al. (2016)
26.	Chemical composition and optical properties	2016/4/12-5/12 2017/7/1-7/31	QOMS, southern TP Waliguan, northeastern TP	$PM_{2.5}$ samples	off-line, 48 h	Xu et al. (2020)
27.	Molecular composition and optical properties of WS-BrC					Xu et al. (2022a)
28.	Characteristics and sources of $PM_{2.5}$	2018/3/11-5/13	Gaomeigu, southeastern TP	$PM_{2.5}$ samples	off-line, 24 h	Zhao et al. (2019b)
29.	Abundance, composition and source of $PM_{2.5}$	2010/7/3-8/26	Qinghai Lake, northeastern TP	$PM_{2.5}$ samples	off-line, 24 h	Li et al. (2013)
30.	Seasonal/diurnal variation of molecular tracers for OAs	2014/12/21-2015/2/1 2015/8/4-9/6	Nam Co, inland TP	TSP samples	off-line, 12 h	Wan et al. (2023)

	Off-line filter sample analysis for aerosol light absorption of CAs (BC/EC/OC/WSOC/BrC/HULIS)					
31.	Light absorption of CAs	2014/8-2015/8	QOMS and Lulang	TSP samples	off-line, 2 samples/month	Li et al. (2016c)
32.	Seasonal variation and light absorption property of CAs	2014/12-2016/12	Mt. Yulong and Ganhaizi basin	TSP samples	off-line, 6 days	Niu et al. (2017)
33.	Light absorption by WSOC	2015/6/2-7/1	Nam Co Station, inland TP	$PM_{2.5}$ samples	off-line, 24 h	Zhang et al. (2017)
34.	Sources and light absorption characteristics of WSOC	2016/11-2017/11	Nam Co, inland TP	$PM_{2.5}$ and TSP samples	off-line	Li et al. (2021b)
35.	Multi-wavelength light absorption of BC and BrC	2008/7/16-2009/7/26	Lulang, southeastern TP	TSP samples	off-line, 72 h	Zhao et al. (2019a)
36.	Light absorption, fluorescence properties and sources of BrC	2013/8-2014/1	Lulang, southeastern TP	TSP samples	off-line, 11.5 h	Wu et al. (2020)
37.	Light absorption properties of BrC	2015/11-2016/11	Lulang, southeastern TP	TSP samples	off-line, weekly	Zhu et al. (2018)
38.	Light absorption of CAs from the Sichuan Basin to TP	2018/12/21-2019/12/18	Six sites from SCB to TP	PM_1 samples	off-line, day/night	Zhao et al. (2022a)
39.	Molecular compositions and light absorption of HULIS	2015/3/22-2015/4/14	Mt. Yulong, southeastern TP	$PM_{2.5}$ samples	off-line, 48 h	Wang et al. (2019b)
	Off-line filter sample analysis for PAHs, Individual particle analysis by TEM, Isotope Analysis, and others					
40.	Concentrations of PAHs	2008/8/5-2009/7/13	Lhasa, urban city	TSP samples	off-line, 24 h/week	Ma et al. (2013)
41.	Source apportionment and risk assessment of atmospheric PAH	2013/4-2014/3	Lhasa, urban city	TSP samples	off-line, 24 h	Chen et al. (2018a)
42.	n-Alkanes and PAHs	2015/11-2016/11	Lulang, southeastern TP	TSP samples	off-line, weekly	Zhu et al. (2020)
43.	Individual particle analysis (Mixing state and sources)	2013/9/15-10/15	Menyuan, northeastern TP	TEM samples	off-line	Li et al. (2015)
44.	Individual particle analysis (Mixing State and Fractal Dimension)	2016/5/26-6/2	Lulang, southeastern TP	TEM samples	off-line	Yuan et al. (2019)
45.	Individual particle analysis (composition and sources)	2013/2/2-3/8	Lhasa, urban city	TEM samples	off-line	Duo et al. (2015)
46.	Radiocarbon and stable isotope ^{13}C of OC and EC	2018/9-2019/8	Qinghai Lake, northeastern TP	TSP samples	off-line, 1 week	Ni et al. (2023)
47.	$\Delta^{14}C$ and $\delta^{13}C$ of TC and IPC	2020/7-2021/6	Hongyuan, eastern TP	$PM_{2.5}$ and TSP samples	off-line, every 2 weeks	Li et al. (2022)
48.	Stable isotope (^{15}N) analysis of nitrogen compounds	2017/3/23-2018/3/19	QOMS, southern TP	TSP samples	off-line	Bhattarai et al. (2023)
49.	Nitrogen and oxygen isotopic compositions	2017/3-2018/2	QOMS, southern TP	TSP samples	off-line, 1 week	Lin et al. (2021)
50.	S-isotope characteristic	2021/3-2021/6	QOMS, southern TP	$PM_{2.5}$ samples	off-line, 96 h	Dasari et al. (2023)
51.	Primary biological aerosol particles (PBAPs)	2018/8-2019/9; 2018/9-2019/7; 2019/7-2020/7	Qinghai lake, Beiluhe, Ngari	TSP samples	off-line	Zhu et al. (2022)
52.	Oxalic acid and related SOA	2010/7-2010/8	Qinghai Lake, northeastern TP	$PM_{2.5}$ samples	off-line, 24 h	Meng et al. (2013)
	On-line measurement of BC concentration and light absorption of BC and BrC by Aethalometers and other optical instruments					
53.	Concentration, temporal variation, and sources of BC	2015/5/15-2017/5/31	QOMS, southern TP	AE-33 Aethalometer	on-line, 1-min	Chen et al. (2018b)
54.	BC concentration	2009/5-2011/3	Qilian Shan, northeastern TP	AE-31 Aethalometer	on-line, 5-min	Zhao et al. (2012)
55.	BC concentration	2008/11-2009/1	Linzhi, southeastern TP	AE-16 Aethalometer	on-line, 5-min	Cao et al. (2011)
56.	Aerosol light absorption	Autumn 2015	Lhasa and Lulang	AE-33 Aethalometer	on-line, 1-min	Zhu et al. (2017)
57.	Light absorption contributions of BC, BrC_{pri}, and BrC_{sec}	2018/8-2019/9; 2018/9-2019/7; 2019/7-2020/7	Qinghai lake, Beiluhe, Ngari	AE-33 Aethalometer	on-line	Zhu et al. (2021)
58.	Secondary BrC absorption	2018/3/14-5/13	Gaomeigu, southeastern TP	AE-33 Aethalometer	on-line, 1-min	Wang et al. (2019a)
59.	Source contribution of fossil fuels and biomass-burning BC	2018/3/14-5/13	Lijiang, southeastern TP	AE33 Aethalometer/PAX	on-line	Liu et al. (2021)
60.	Mass concentrations, size distributions, mixing states, and light absorption properties of refractory BC	2015/9/17-10/31	Lulang, southeastern TP	SP2 and PAX	on-line, hourly	Wang et al. (2018)

61.	Light absorption properties of BC and BrC	2015/5/31-7/1 2016/4/12-5/12 2017/7/1-7/31	Nam Co, inland TP QOMS, southern TP Waliguan, northeastern TP	Aethalometer PAX/MAAP HR-ToF-AMS	on-line, 5-min on-line, hourly	Zhang et al. (2021b)
62.	Optical properties, size distributions, chemical compositions	2019/7/8-8/2	Shiquanhe, southwestern TP	Nephelometer/PAX/APS	on-line, 10s-5 min	Zhang et al. (2021a)
63.	Optical characteristics of aerosol	2020/8/5-9/11	Nam Co, inland TP	APS/MAPP	on-line, 5/1-min	Wang et al. (2023)
	On-line measurement of aerosol mass and number concentrations by TEOM RP1400, SMPS, and other instruments					
64.	Concentrations of BC, $PM_{2.5}$, PM_{10}, and CAs and WSIs	2004/4/7-5/24	Tengchong, southeastern TP	TEOM RP1400/Aethalometer $PM_{2.5}$ and PM_{10} samples	on-line, 5-min off-line, 24-48 h	Engling et al. (2011)
65.	Characteristics of aerosol mass loadings	2011–2013	Ngari, QOMS, Nam Co, SET	TEOM RP1400 $PM_{2.5}$ samples	on-line, 5-min off-line, 3 days	Liu et al. (2017)
66.	Spatial and temporal variations of particulate pollutants	2016/6-2017/5	Lhasa, Ngari, Qamdo, Nyingchi, Nagchu, and Shigatse	CNEMC download data	on-line, hourly	Chen et al. (2019b)
67.	New particle formation	2019/4/26-5/22 2019/6/15-6/25	Nam Co, inland TP	SMPSs AE-33 Aethalometer	on-line	Tang et al. (2022)
68.	Vertical profiling of particle size distributions	2020/8/8-8/28	Lhasa, urban city	POPS and GRIMM 11-C attached to a tethered balloon	on-line	Ran et al. (2022)
69.	Aerosol number size distribution	2016/8/2-8/20	Lhasa, urban city	Optical particle size spectrometer	on-line, 10-min	Cui et al. (2018)
70.	First simultaneous measurements of PAN and O_3	summer in 2011/2012	Nam Co, inland TP	PAN Analyzer	on-line, 10-min	Xu et al. (2018b)
71.	Measurements of O_3 and PAN as well as their precursors	2019/5/1-7/31	Nam Co, inland TP	GC-ECD analyzer	on-line	Xu et al. (2023)
	On-line measurement of ambient aerosol chemical composition by aerosol mass spectrometers					
72.	Chemical characterization of PM_1	2013/9/5-10/15	Menyuan, northeastern TP	ACSM	on-line, 15-min	Du et al. (2015)
73.	Chemical composition of PM_1	2015/3/22-4/14	Mt. Yulong, southeastern TP	HR-ToF-AMS	on-line, 5-min	Zheng et al. (2017)
74.	Chemical characterization of rBC	2015/5/30-6/30	Nam Co, inland TP	SP-AMS/HR-ToF-AMS MAAP	on-line, 5-min	Wang et al. (2017)
75.	Chemical characteristics and sources of PM_1	2015/5/31-7/1	Nam Co, inland TP	HR-ToF-AMS/SMPS/MAAP etc.	on-line, 5-min	Xu et al. (2018a)
76.	Chemical characteristics and sources of PM_1	2016/4/12-5/12	QOMS, southern TP	HR-ToF-AMS/SMPS/PAX	on-line, 5-min	Zhang et al. (2018)
77.	Chemical characteristics and sources of PM_1	2017/7/1-7/31	Waliguan, northeastern TP	HR-ToF-AMS/PAX/CCN-100	on-line, 10-min	Zhang et al. (2019)
78.	Chemical characteristics and sources of PM_1 during a festival	2017/7/5-7/6	Waliguan, northeastern TP	HR-ToF-AMS/PAX/CCN-100	on-line, 10-min	Zhang et al. (2020)
79.	Chemical characteristics and sources of PM_1	2019/8/31-9/26	Lhasa, urban city	HR-ToF-AMS/SMPS/PAX	on-line, 5-min	Zhao et al. (2022b)
80.	Regional difference of aerosol chemical compositions and sources in the TP and its surroundings	Different periods during 2015-2022	QOMS, Motuo, NamCo, Ngari, Waliguan, LHG, Bayanbulak, and Lhasa	HR-ToF-AMS SMPS/ /CCN-100 PAX/Aethalometer	on-line, hourly	This study

Abbreviation: BC: black carbon; OC: organic carbon; EC: elemental carbon; CAs: carbonaceous aerosols; WSOC: water soluble organic carbon; BrC: brown carbon; WSIs: water soluble ionic species; HULIS: Humic-Like Substances; SOA: secondary organic aerosol; TEM: Transmission electron microscopy; TC: total carbon; IPC: water-insoluble particulate carbon; PAH: polycyclic aromatic hydrocarbons; PAN: peroxyacetyl nitrate; APCC: Atmospheric Pollution and Cryospheric Change; CNEMC: China National Environmental Monitoring Center;

Figures

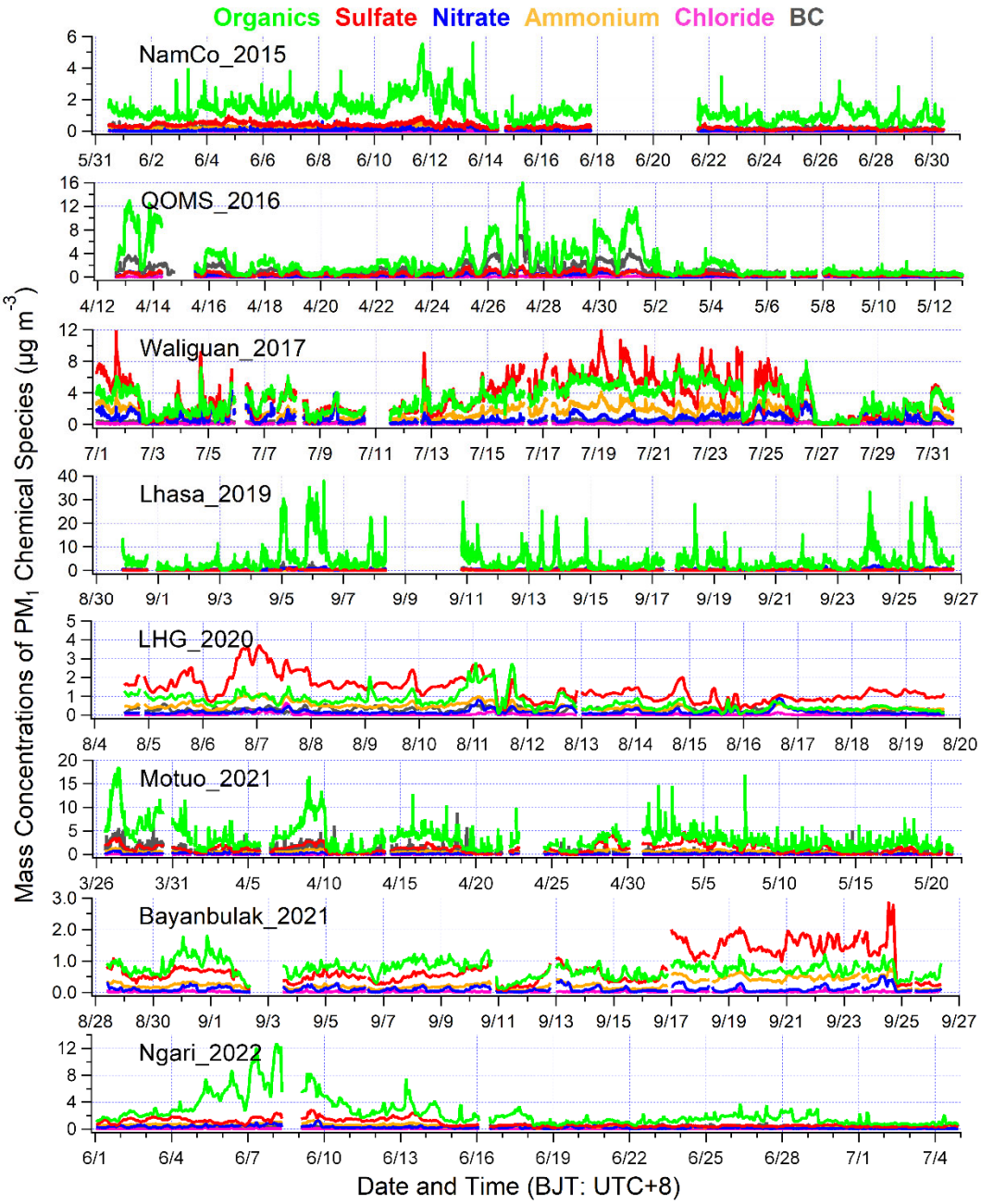

Fig. S1 High-time-resolution temporal variations of the mass concentrations of PM_1 chemical compositions during the eight online aerosol field measurement campaigns over the Tibetan Plateau and its surroundings.

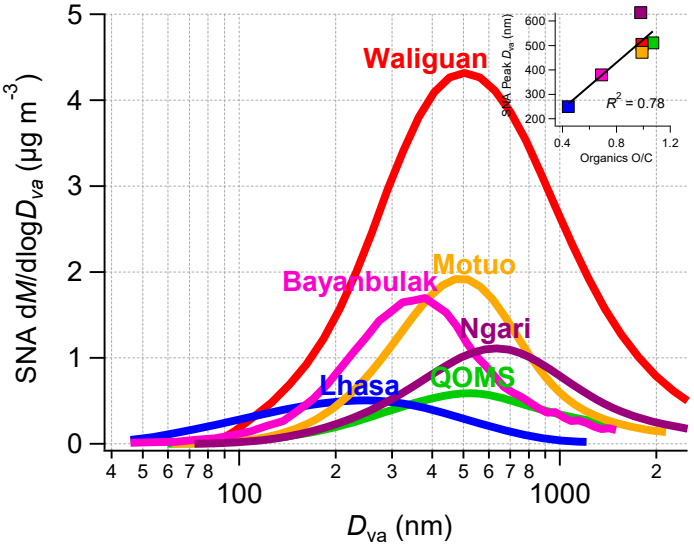

Fig. S2 Average size distributions of SNA mass concentrations during six field measurement campaigns in the Tibetan Plateau and its surroundings. Insert graph is the scatter plot of peak diameters in these size distributions versus the average O/C ratio of organics.

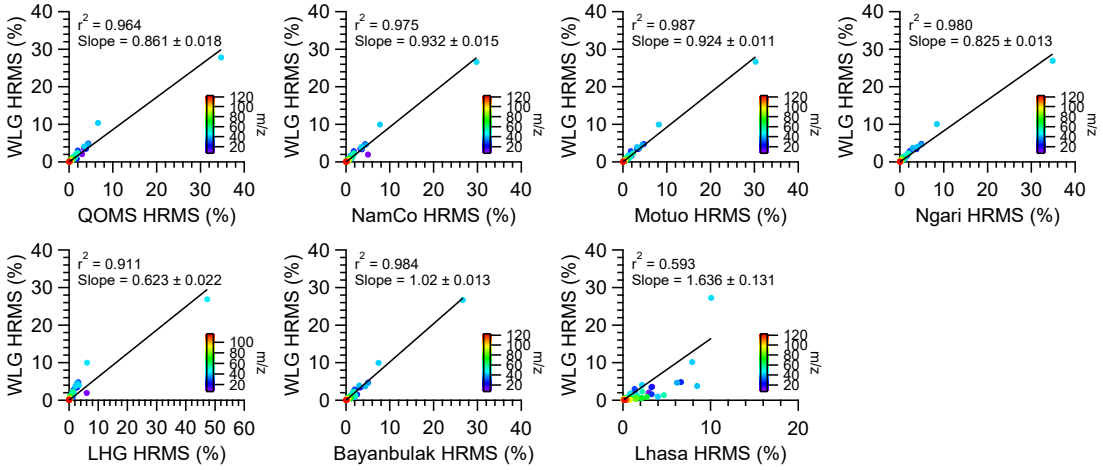

Fig. S3 Comparison of OA HRMS between Waliguan and the other seven sites in this study.

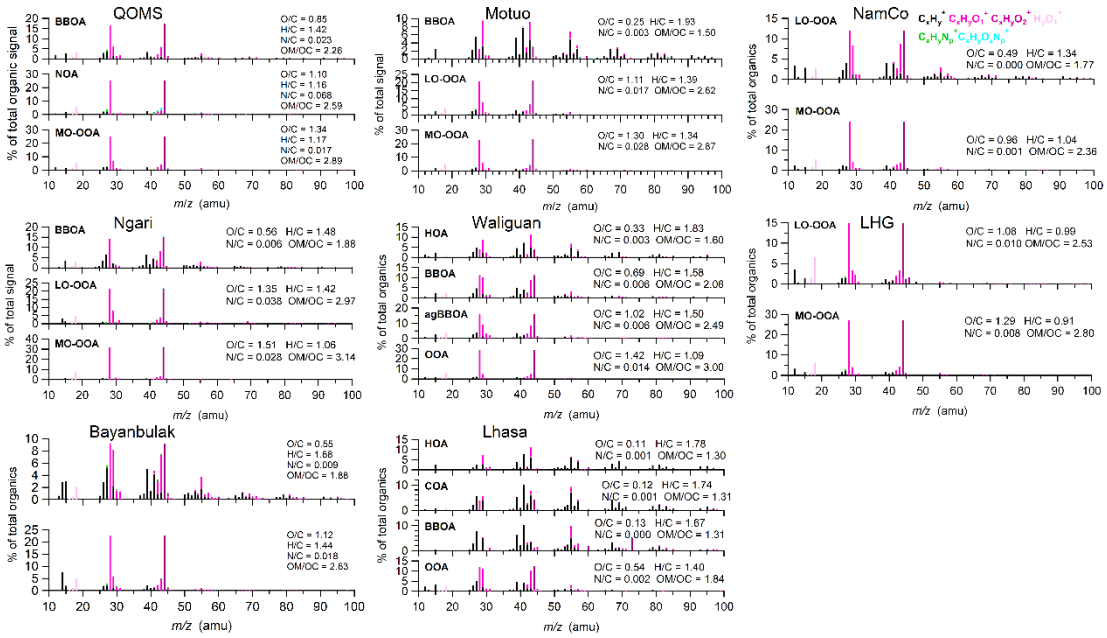

250

251 **Fig. S4** The high-resolution mass spectra (HRMS) of different OA factors identified by the PMF
252 source apportionment among the eight field campaigns in our study. All the HRMSs are colored by
253 six ion categories at m/z < 120.

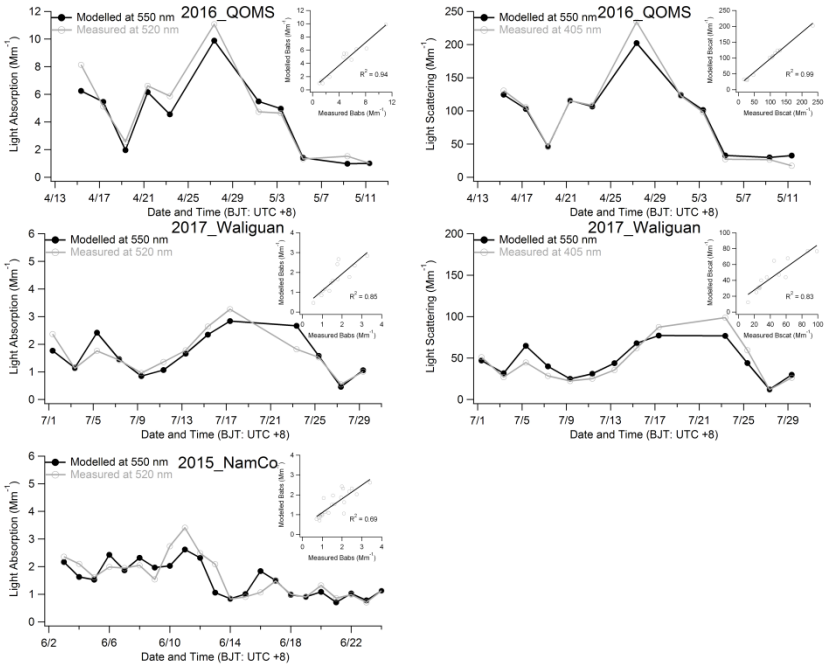

254

255 **Fig. S5** Comparisons of the particle light scattering and absorption coefficients between the
256 modelled values (final selected) from Optical Properties of Aerosol and Cloud (OPAC) model and
257 measured values from the photoacoustic extinctiometer and aethalometer during the three
258 campaigns.

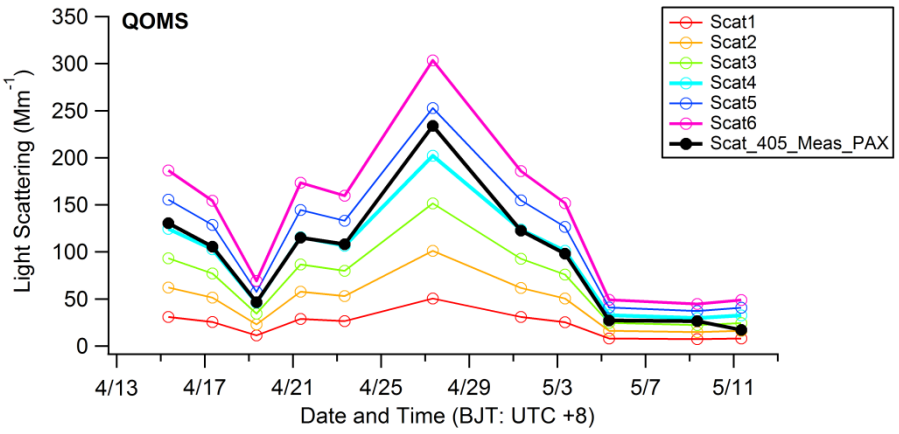

Fig. S6 Time series of the particle light scattering coefficients at 405 nm measured by the PAX and those modelled light scattering coefficients at 550 nm under different particle numbers in per cubic meter air (the calculated value multiplier 1 to 6, respectively) from the OPAC model during the QOMS campaign.

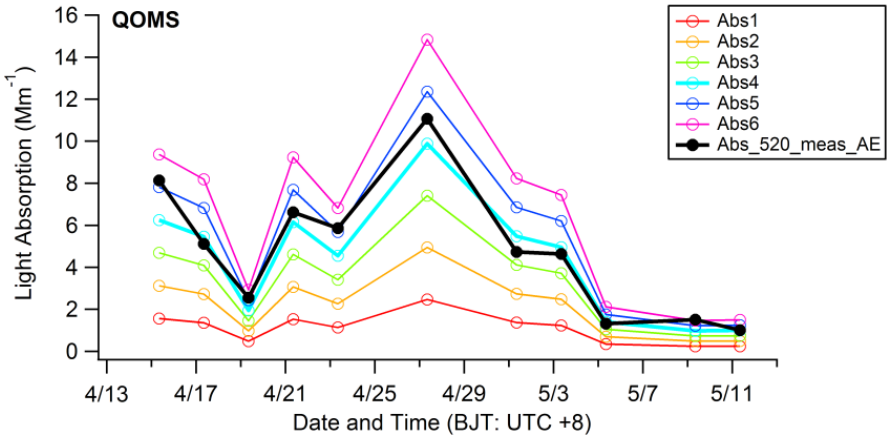

Fig. S7 Time series of the particle light absorption coefficients at 520 nm measured by the Aethalometer and those modelled light absorption coefficients at 550 nm under different particle numbers in per cubic meter air (the calculated value multiplier 1 to 6, respectively) from the OPAC model during the QOMS campaign.

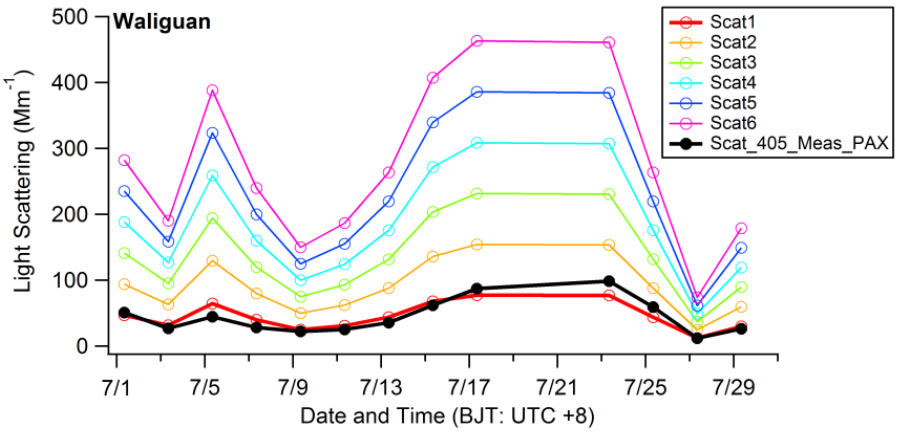

Fig. S8 Time series of the particle light scattering coefficients at 405 nm measured by the PAX and those modelled light scattering coefficients at 550 nm under different particle numbers in per cubic meter air (the calculated value multiplier 1 to 6, respectively) from the OPAC model during the Waliguan campaign.

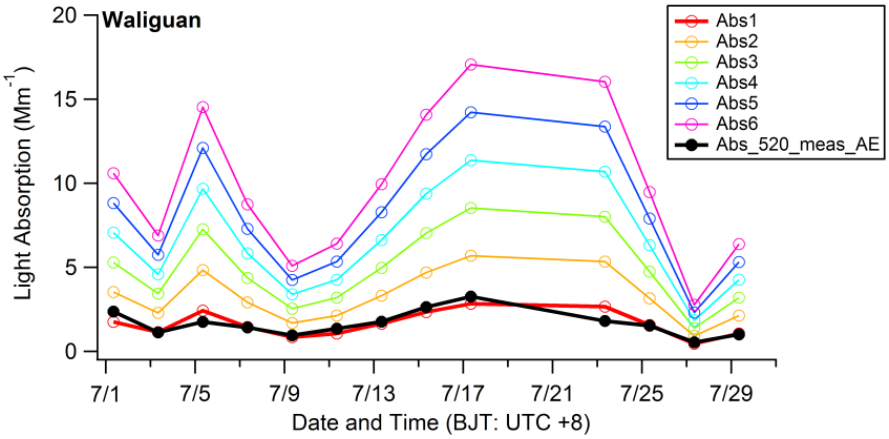

Fig. S9 Time series of the particle light absorption coefficients at 520 nm measured by the Aethalometer and those modelled light absorption coefficients at 550 nm under different particle numbers in per cubic meter air (the calculated value multiplier 1 to 6, respectively) from the OPAC model during the Waliguan campaign.

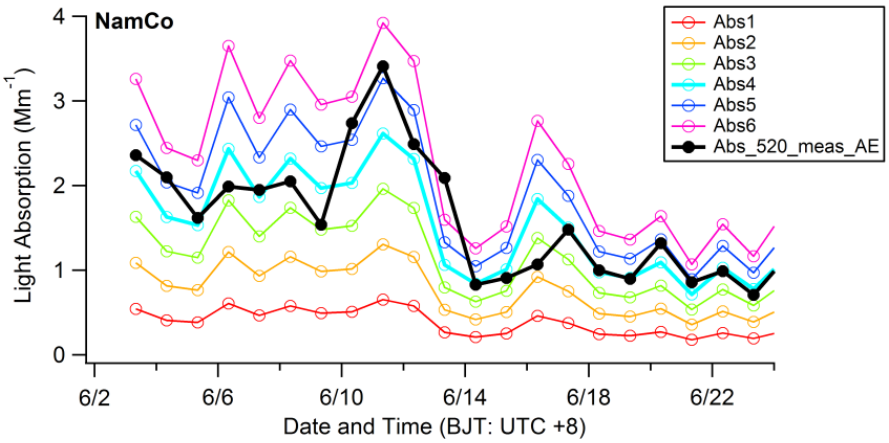

279

280 **Fig. S10** Time series of the particle light absorption coefficients at 520 nm measured by the
281 Aethalometer and those modelled light absorption coefficients at 550 nm under different particle
282 numbers in per cubic meter air (the calculated value multiplier 1 to 6, respectively) from the OPAC
283 model during the NamCo campaign.

References

Aiken, A. C., DeCarlo, P. F., Kroll, J. H., Worsnop, D. R., Huffman, J. A., Docherty, K. S., Ulbrich, I. M., Mohr, C., Kimmel, J. R., Sueper, D., Sun, Y., Zhang, Q., Trimborn, A., Northway, M., Ziemann, P. J., Canagaratna, M. R., Onasch, T. B., Alfarra, M. R., Prevot, A. S. H., Dommen, J., Duplissy, J., Metzger, A., Baltensperger, U., and Jimenez, J. L.: O/C and OM/OC ratios of primary, secondary, and ambient organic aerosols with high-resolution time-of-flight aerosol mass spectrometry, Environ. Sci. Technol., 42, 4478-4485, 10.1021/es703009q, 2008.

Allan, J. D., Delia, A. E., Coe, H., Bower, K. N., Alfarra, M. R., Jimenez, J. L., Middlebrook, A. M., Drewnick, F., Onasch, T. B., Canagaratna, M. R., Jayne, J. T., and Worsnop, D. R.: A generalised method for the extraction of chemically resolved mass spectra from Aerodyne aerosol mass spectrometer data, J. Aerosol Sci., 35, 909-922, 10.1016/j.jaerosci.2004.02.007, 2004.

Bhattarai, H., Wu, G., Zheng, X., Zhu, H., Gao, S., Zhang, Y. L., Widory, D., Ram, K., Chen, X., Wan, X., Pei, Q., Pan, Y., Kang, S., and Cong, Z.: Wildfire-Derived Nitrogen Aerosols Threaten the Fragile Ecosystem in Himalayas and Tibetan Plateau, Environ Sci Technol, 10.1021/acs.est.3c01541, 2023.

Canagaratna, M. R., Jimenez, J. L., Kroll, J. H., Chen, Q., Kessler, S. H., Massoli, P., Hildebrandt Ruiz, L., Fortner, E., Williams, L. R., Wilson, K. R., Surratt, J. D., Donahue, N. M., Jayne, J. T., and Worsnop, D. R.: Elemental ratio measurements of organic compounds using aerosol mass spectrometry: characterization, improved calibration, and implications, Atmos. Chem. Phys., 15, 253-272, 10.5194/acp-15-253-2015, 2015.

Cao, J., Tie, X., Xu, B., Zhao, Z., Zhu, C., Li, G., and Liu, S.: Measuring and modeling black carbon (BC) contamination in the SE Tibetan Plateau, J. Atmos. Chem., 67, 45-60, 10.1007/s10874-011-9202-5, 2011.

Chen, P., Kang, S., Li, C., Li, Q., Yan, F., Guo, J., Ji, Z., Zhang, Q., Hu, Z., Tripathee, L., and Sillanpää, M.: Source Apportionment and Risk Assessment of Atmospheric Polycyclic Aromatic Hydrocarbons in Lhasa, Tibet, China, Aerosol Air Qual. Res., 18, 1294-1304, 10.4209/aaqr.2017.12.0603, 2018a.

Chen, P., Kang, S., Li, C., Zhang, Q., Guo, J., Tripathee, L., Zhang, Y., Li, G., Gul, C., Cong, Z., Wan, X., Niu, H., Panday, A. K., Rupakheti, M., and Ji, Z.: Carbonaceous aerosol characteristics on the Third Pole: A primary study based on the Atmospheric Pollution and Cryospheric Change (APCC) network, Environ. Pollut., 253, 49-60, 10.1016/j.envpol.2019.06.112, 2019a.

Chen, P., Yang, J., Pu, T., Li, C., Guo, J., Tripathee, L., and Kang, S.: Spatial and Temporal Variations of Gaseous and Particulate Pollutants in Six Sites in Tibet, China, during 2016–2017, Aerosol Air Qual. Res., 19, 516-527, 10.4209/aaqr.2018.10.0360, 2019b.

Chen, X., Kang, S., Cong, Z., Yang, J., and Ma, Y.: Concentration, temporal variation, and sources of black carbon in the Mt. Everest region retrieved by real-time observation and simulation, Atmos. Chem. Phys., 18, 12859-12875, 10.5194/acp-18-12859-2018, 2018b.

Cong, Z., Kang, S., Kawamura, K., Liu, B., Wan, X., Wang, Z., Gao, S., and Fu, P.: Carbonaceous aerosols on the south edge of the Tibetan Plateau: concentrations, seasonality and sources, Atmos. Chem. Phys., 15, 1573-1584, 10.5194/acp-15-1573-2015, 2015.

Cui, Y. Y., Liu, S., Bai, Z., Bian, J., Li, D., Fan, K., McKeen, S. A., Watts, L. A., Ciciora, S. J., and Gao, R.-S.: Religious burning as a potential major source of atmospheric fine aerosols in summertime Lhasa on the Tibetan Plateau, Atmos. Environ., 181, 186-191, 10.1016/j.atmosenv.2018.03.025, 2018.

Dasari, S., Paris, G., Pei, Q., Cong, Z., and Widory, D.: Tracing the origin of elevated springtime atmospheric sulfate on the Southern Himalayan-Tibetan Plateau, Environmental Science: Advances,

10.1039/d3va00085k, 2023.

DeCarlo, P. F., Kimmel, J. R., Trimborn, A., Northway, M. J., Jayne, J. T., Aiken, A. C., Gonin, M., Fuhrer, K., Horvath, T., Docherty, K. S., Worsnop, D. R., and Jimenez, J. L.: Field-Deployable, High-Resolution, Time-of-Flight Aerosol Mass Spectrometer, Anal. Chem., 78, 8281-8289, 10.1021/ac061249n, 2006.

Du, W., Sun, Y. L., Xu, Y. S., Jiang, Q., Wang, Q. Q., Yang, W., Wang, F., Bai, Z. P., Zhao, X. D., and Yang, Y. C.: Chemical characterization of submicron aerosol and particle growth events at a national background site (3295 m a.s.l.) on the Tibetan Plateau, Atmos. Chem. Phys., 15, 10811-10824, 10.5194/acp-15-10811-2015, 2015.

Duo, B., Zhang, Y., Kong, L., Fu, H., Hu, Y., Chen, J., Li, L., and Qiong, A.: Individual particle analysis of aerosols collected at Lhasa City in the Tibetan Plateau, J Environ Sci (China), 29, 165-177, 10.1016/j.jes.2014.07.032, 2015.

Engling, G., Zhang, Y. N., Chan, C. Y., Sang, X. F., Lin, M., Ho, K. F., Li, Y. S., Lin, C. Y., and Lee, J. J.: Characterization and sources of aerosol particles over the southeastern Tibetan Plateau during the Southeast Asia biomass-burning season, Tellus B: Chemical and Physical Meteorology, 63, 117-128, 10.1111/j.1600-0889.2010.00512.x, 2011.

Gong, C., Xin, J., Wang, S., Wang, Y., and Zhang, T.: Anthropogenic aerosol optical and radiative properties in the typical urban/suburban regions in China, Atmos. Res., 197, 177-187, 10.1016/j.atmosres.2017.07.002, 2017.

Hess, M., Koepke, P., and Schult, I.: Optical Properties of Aerosols and Clouds: The Software Package OPAC, Bull. Am. Meteorol. Soc., 79, 831-844, 10.1175/1520-0477(1998)079<0831:OPOAAC>2.0.CO;2, 1998.

Hu, Z., Kang, S., Xu, J., Zhang, C., Li, X., Yan, F., Zhang, Y., Chen, P., and Li, C.: Significant overestimation of black carbon concentration caused by high organic carbon in aerosols of the Tibetan Plateau, Atmos. Environ., 294, 10.1016/j.atmosenv.2022.119486, 2023.

Jayne, J. T., Leard, D. C., Zhang, X. F., Davidovits, P., Smith, K. A., Kolb, C. E., and Worsnop, D. R.: Development of an aerosol mass spectrometer for size and composition analysis of submicron particles, Aerosol Sci. Technol., 33, 49-70, 10.1080/027868200410840, 2000.

Jimenez, J. L., Jayne, J. T., Shi, Q., Kolb, C. E., Worsnop, D. R., Yourshaw, I., Seinfeld, J. H., Flagan, R. C., Zhang, X., Smith, K. A., Morris, J. W., and Davidovits, P.: Ambient aerosol sampling using the Aerodyne Aerosol Mass Spectrometer, J. Geophys. Res., 108, 8425, 10.1029/2001jd001213, 2003.

Kang, S., Chen, P., Li, C., Liu, B., and Cong, Z.: Atmospheric Aerosol Elements over the Inland Tibetan Plateau: Concentration, Seasonality, and Transport, Aerosol Air Qual. Res., 16, 789-800, 10.4209/aaqr.2015.05.0307, 2016.

Kang, S., Zhang, Y., Chen, P., Guo, J., Zhang, Q., Cong, Z., Kaspari, S., Tripathee, L., Gao, T., Niu, H., Zhong, X., Chen, X., Hu, Z., Li, X., Li, Y., Neupane, B., Yan, F., Rupakheti, D., Gul, C., Zhang, W., Wu, G., Yang, L., Wang, Z., and Li, C.: Black carbon and organic carbon dataset over the Third Pole, Earth System Science Data, 14, 683-707, 10.5194/essd-14-683-2022, 2022.

Li, C., Bosch, C., Kang, S., Andersson, A., Chen, P., Zhang, Q., Cong, Z., Chen, B., Qin, D., and Gustafsson, O.: Sources of black carbon to the Himalayan-Tibetan Plateau glaciers, Nat. Commun., 7, 12574, 10.1038/ncomms12574, 2016a.

Li, C., Chen, P., Kang, S., Yan, F., Hu, Z., Qu, B., and Sillanpää, M.: Concentrations and light absorption characteristics of carbonaceous aerosol in PM2.5 and PM10 of Lhasa city, the Tibetan Plateau, Atmos. Environ., 127, 340-346, https://doi.org/10.1016/j.atmosenv.2015.12.059, 2016b.

Li, C., Yan, F., Kang, S., Chen, P., Hu, Z., Gao, S., Qu, B., and Sillanpää, M.: Light absorption characteristics of carbonaceous aerosols in two remote stations of the southern fringe of the Tibetan Plateau, China, Atmos. Environ., 143, 79-85, 10.1016/j.atmosenv.2016.08.042, 2016c.

Li, C., Han, X., Kang, S., Yan, F., Chen, P., Hu, Z., Yang, J., Ciren, D., Gao, S., Sillanpaa, M., Han, Y., Cui, Y., Liu, S., and Smith, K. R.: Heavy near-surface PM(2.5) pollution in Lhasa, China during a relatively static winter period, Chemosphere, 214, 314-318, 10.1016/j.chemosphere.2018.09.135, 2019.

Li, C., Yan, F., Kang, S., Yan, C., Hu, Z., Chen, P., Gao, S., Zhang, C., He, C., Kaspari, S., and Stubbins, A.: Carbonaceous matter in the atmosphere and glaciers of the Himalayas and the Tibetan plateau: An investigative review, Environ Int, 146, 106281, 10.1016/j.envint.2020.106281, 2021a.

Li, C., Zhang, C., Yan, F., Kang, S., Xu, Y., Liu, Y., Gao, Y., Chen, P., and He, C.: Importance of local non-fossil sources to carbonaceous aerosols at the eastern fringe of the Tibetan Plateau, China: Delta(14)C and delta(13)C evidences, Environ Pollut, 119858, 10.1016/j.envpol.2022.119858, 2022.

Li, J., Wang, G., Wang, X., Cao, J., Sun, T., Cheng, C., Meng, J., Hu, T., and Liu, S.: Abundance, composition and source of atmospheric PM2.5 at a remote site in the Tibetan Plateau, China, Tellus B: Chemical and Physical Meteorology, 65, 20281, 10.3402/tellusb.v65i0.20281, 2013.

Li, W. J., Chen, S. R., Xu, Y. S., Guo, X. C., Sun, Y. L., Yang, X. Y., Wang, Z. F., Zhao, X. D., Chen, J. M., and Wang, W. X.: Mixing state and sources of submicron regional background aerosols in the northern Qinghai–Tibet Plateau and the influence of biomass burning, Atmos. Chem. Phys., 15, 13365-13376, 10.5194/acp-15-13365-2015, 2015.

Li, Y., Yan, F., Kang, S., Zhang, C., Chen, P., Hu, Z., and Li, C.: Sources and light absorption characteristics of water-soluble organic carbon (WSOC) of atmospheric particles at a remote area in inner Himalayas and Tibetan Plateau, Atmos. Res., 253, 105472, 10.1016/j.atmosres.2021.105472, 2021b.

Lin, Y. C., Zhang, Y. L., Yu, M., Fan, M. Y., Xie, F., Zhang, W. Q., Wu, G., Cong, Z., and Michalski, G.: Formation Mechanisms and Source Apportionments of Airborne Nitrate Aerosols at a Himalayan-Tibetan Plateau Site: Insights from Nitrogen and Oxygen Isotopic Compositions, Environ Sci Technol, 55, 12261-12271, 10.1021/acs.est.1c03957, 2021.

Liu, B., Cong, Z., Wang, Y., Xin, J., Wan, X., Pan, Y., Liu, Z., Wang, Y., Zhang, G., Wang, Z., Wang, Y., and Kang, S.: Background aerosol over the Himalayas and Tibetan Plateau: observed characteristics of aerosol mass loading, Atmos. Chem. Phys., 17, 449-463, 10.5194/acp-17-449-2017, 2017.

Liu, H., Wang, Q., Xing, L., Zhang, Y., Zhang, T., Ran, W., and Cao, J.: Measurement report: quantifying source contribution of fossil fuels and biomass-burning black carbon aerosol in the southeastern margin of the Tibetan Plateau, Atmos. Chem. Phys., 21, 973-987, 10.5194/acp-21-973-2021, 2021.

Ma, W. L., Qi, H., Baidron, S., Liu, L. Y., Yang, M., and Li, Y. F.: Implications for long-range atmospheric transport of polycyclic aromatic hydrocarbons in Lhasa, China, Environmental science and pollution research international, 20, 5525-5533, 10.1007/s11356-013-1577-1, 2013.

Meng, J., Wang, G., Li, J., Cheng, C., and Cao, J.: Atmospheric oxalic acid and related secondary organic aerosols in Qinghai Lake, a continental background site in Tibet Plateau, Atmos. Environ., 79, 582-589, 10.1016/j.atmosenv.2013.07.024, 2013.

Meng, Y., Li, R., Zhao, Y., Cheng, H., Fu, H., Yan, Z., and Bing, H.: Chemical characterization and sources of PM2.5 at a high-alpine ecosystem in the Southeast Tibetan Plateau, China, Atmos. Environ., 235, 117645, 10.1016/j.atmosenv.2020.117645, 2020.

Middlebrook, A. M., Bahreini, R., Jimenez, J. L., and Canagaratna, M. R.: Evaluation of Composition-

Dependent Collection Efficiencies for the Aerodyne Aerosol Mass Spectrometer using Field Data, Aerosol Sci. Technol., 46, 258-271, 10.1080/02786826.2011.620041, 2012.

Ni, H., Yao, P., Zhu, C., Qu, Y., Tian, J., Ma, Y., Yang, L., Zhong, H., Huang, R. J., and Dusek, U.: Non-Fossil Origin Explains the Large Seasonal Variation of Highly Processed Organic Aerosol in the Northeastern Tibetan Plateau (3,200 m a.s.l.), Geophys. Res. Lett., 50, 10.1029/2023gl104710, 2023.

Niu, H., Kang, S., Wang, H., Zhang, R., Lu, X., Qian, Y., Wang, S., Paudyal, R., Shi, X., and Yan, X.: Spatio-temporal variability and light absorption property of carbonaceous aerosol in a typical glacierization region of the Tibetan Plateau, Atmospheric Chemistry and Physics Discussions, 1-43, 10.5194/acp-2017-865, 2017.

Paatero, P., and Tapper, U.: Positive matrix factorization: A non-negative factor model with optimal utilization of error estimates of data values, Environmetrics, 5, 111-126, 10.1002/env.3170050203, 1994.

Ran, L., Deng, Z., Wu, Y., Li, J., Bai, Z., Lu, Y., Zhuoga, D., and Bian, J.: Measurement report: Vertical profiling of particle size distributions over Lhasa, Tibet – tethered balloon-based in situ measurements and source apportionment, Atmos. Chem. Phys., 22, 6217-6229, 10.5194/acp-22-6217-2022, 2022.

Ricchiazzi, P., Yang, S., Gautier, C., and Sowle, D.: SBDART: A Research and Teaching Software Tool for Plane-Parallel Radiative Transfer in the Earth's Atmosphere, Bull. Am. Meteorol. Soc., 79, 2101-2114, 10.1175/1520-0477(1998)079<2101:Sarats>2.0.Co;2, 1998.

Roberts, G. C., and Nenes, A.: A Continuous-Flow Streamwise Thermal-Gradient CCN Chamber for Atmospheric Measurements, Aerosol Science and Technology, 39, 206-221, 10.1080/027868290913988, 2005.

Schueneman, M. K., Nault, B. A., Campuzano-Jost, P., Jo, D. S., Day, D. A., Schroder, J. C., Palm, B. B., Hodzic, A., Dibb, J. E., and Jimenez, J. L.: Aerosol pH indicator and organosulfate detectability from aerosol mass spectrometry measurements, Atmos. Meas. Tech., 14, 2237-2260, 10.5194/amt-14-2237-2021, 2021.

Su, H.-J., Xin, J.-Y., Ma, Y.-J., Liu, Z., Wen, T.-X., Wang, S.-G., Fan, G.-Z., Li, W., Wang, L., He, Z.-M., and Wang, Y.-S.: Effects of transport on aerosols over the eastern slope of the Tibetan Plateau: synergistic contribution of Southeast Asia and the Sichuan Basin, Atmospheric and Oceanic Science Letters, 11, 425-431, 10.1080/16742834.2018.1512832, 2018.

Tang, L., Hu, M., Shang, D., Fang, X., Mao, J., Xu, W., Zhou, J., Zhao, W., Wang, Y., Zhang, C., Zhang, Y., Hu, J., Zeng, L., Ye, C., Guo, S., and Wu, Z.: High frequency of new particle formation events driven by summer monsoon in the central Tibetan Plateau, China, 10.5194/acp-2022-440, 2022.

Ulbrich, I. M., Canagaratna, M. R., Zhang, Q., Worsnop, D. R., and Jimenez, J. L.: Interpretation of organic components from Positive Matrix Factorization of aerosol mass spectrometric data, Atmos. Chem. Phys., 9, 2891-2918, 10.5194/acp-9-2891-2009, 2009.

Wan, X., Kang, S., Wang, Y., Xin, J., Liu, B., Guo, Y., Wen, T., Zhang, G., and Cong, Z.: Size distribution of carbonaceous aerosols at a high-altitude site on the central Tibetan Plateau (Nam Co Station, 4730ma.s.l.), Atmos. Res., 153, 155-164, 10.1016/j.atmosres.2014.08.008, 2015.

Wan, X., Kang, S., Xin, J., Liu, B., Wen, T., Wang, P., Wang, Y., and Cong, Z.: Chemical composition of size-segregated aerosols in Lhasa city, Tibetan Plateau, Atmos. Res., 174-175, 142-150, 10.1016/j.atmosres.2016.02.005, 2016.

Wan, X., Fu, P., Kang, S., Kawamura, K., Wu, G., Li, Q., Gao, S., and Cong, Z.: Organic aerosols in the inland Tibetan Plateau: New insights from molecular tracers, Science of the Total Environment, 884, 163797, 10.1016/j.scitotenv.2023.163797, 2023.

Wang, J., Zhang, Q., Chen, M., Collier, S., Zhou, S., Ge, X., Xu, J., Shi, J., Xie, C., Hu, J., Ge, S., Sun, Y., and Coe, H.: First Chemical Characterization of Refractory Black Carbon Aerosols and Associated Coatings over the Tibetan Plateau (4730 m a.s.l), Environ. Sci. Technol., 51, 14072-14082, 10.1021/acs.est.7b03973, 2017.

Wang, J., Cao, X., Li, M., Tang, C., Zhang, Z., Zhang, H., Tian, P., Liang, J., Zhang, L., and Shi, J.: Optical characteristics of aerosol and its potential sources over Nam Co in the Tibetan Plateau during Asian summer monsoon period, Atmos. Environ., 298, 10.1016/j.atmosenv.2023.119611, 2023.

Wang, Q., Cao, J., Han, Y., Tian, J., Zhu, C., Zhang, Y., Zhang, N., Shen, Z., Ni, H., Zhao, S., and Wu, J.: Sources and physicochemical characteristics of black carbon aerosol from the southeastern Tibetan Plateau: internal mixing enhances light absorption, Atmos. Chem. Phys., 18, 4639-4656, 10.5194/acp-18-4639-2018, 2018.

Wang, Q., Han, Y., Ye, J., Liu, S., Pongpiachan, S., Zhang, N., Han, Y., Tian, J., Wu, C., Long, X., Zhang, Q., Zhang, W., Zhao, Z., and Cao, J.: High Contribution of Secondary Brown Carbon to Aerosol Light Absorption in the Southeastern Margin of Tibetan Plateau, Geophys. Res. Lett., 46, 4962-4970, 10.1029/2019gl082731, 2019a.

Wang, Y., Hu, M., Lin, P., Tan, T., Li, M., Xu, N., Zheng, J., Du, Z., Qin, Y., Wu, Y., Lu, S., Song, Y., Wu, Z., Guo, S., Zeng, L., Huang, X., and He, L.: Enhancement in Particulate Organic Nitrogen and Light Absorption of Humic-Like Substances over Tibetan Plateau Due to Long-Range Transported Biomass Burning Emissions, Environ. Sci. Technol., 53, 14222-14232, 10.1021/acs.est.9b06152, 2019b.

Wei, N., Ma, C., Liu, J., Wang, G., Liu, W., Zhuoga, D., Xiao, D., and Yao, J.: Size-Segregated Characteristics of Carbonaceous Aerosols during the Monsoon and Non-Monsoon Seasons in Lhasa in the Tibetan Plateau, Atmosphere, 10, 10.3390/atmos10030157, 2019a.

Wei, N., Xu, Z., Liu, J., Wang, G., Liu, W., Zhuoga, D., Xiao, D., and Yao, J.: Characteristics of size distributions and sources of water-soluble ions in Lhasa during monsoon and non-monsoon seasons, J Environ Sci (China), 82, 155-168, 10.1016/j.jes.2019.02.017, 2019b.

Wu, G., Wan, X., Gao, S., Fu, P., Yin, Y., Li, G., Zhang, G., Kang, S., Ram, K., and Cong, Z.: Humic-Like Substances (HULIS) in Aerosols of Central Tibetan Plateau (Nam Co, 4730 m asl): Abundance, Light Absorption Properties, and Sources, Environ. Sci. Technol., 52, 7203-7211, 10.1021/acs.est.8b01251, 2018.

Wu, G., Wan, X., Ram, K., Li, P., Liu, B., Yin, Y., Fu, P., Loewen, M., Gao, S., Kang, S., Kawamura, K., Wang, Y., and Cong, Z.: Light absorption, fluorescence properties and sources of brown carbon aerosols in the Southeast Tibetan Plateau, Environ. Pollut., 257, 113616, 10.1016/j.envpol.2019.113616, 2020.

Xin, J., Gong, C., Wang, S., and Wang, Y.: Aerosol direct radiative forcing in desert and semi-desert regions of northwestern China, Atmos. Res., 171, 56-65, 10.1016/j.atmosres.2015.12.004, 2016.

Xu, J., Wang, Z., Yu, G., Qin, X., Ren, J., and Qin, D.: Characteristics of water soluble ionic species in fine particles from a high altitude site on the northern boundary of Tibetan Plateau: Mixture of mineral dust and anthropogenic aerosol, Atmos. Res., 143, 43-56, 10.1016/j.atmosres.2014.01.018, 2014.

Xu, J., Zhang, Q., Wang, Z. B., Yu, G. M., Ge, X. L., and Qin, X.: Chemical composition and size distribution of summertime $PM_{2.5}$ at a high altitude remote location in the northeast of the Qinghai-Xizang (Tibet) Plateau: insights into aerosol sources and processing in free troposphere, Atmos. Chem. Phys., 15, 5069-5081, 10.5194/acp-15-5069-2015, 2015.

Xu, J., Zhang, Q., Shi, J., Ge, X., Xie, C., Wang, J., Kang, S., Zhang, R., and Wang, Y.: Chemical characteristics of submicron particles at the central Tibetan Plateau: insights from aerosol mass

spectrometry, Atmos. Chem. Phys., 18, 427-443, 10.5194/acp-18-427-2018, 2018a.

Xu, J., Hettiyadura, A. P. S., Liu, Y., Zhang, X., Kang, S., and Laskin, A.: Regional Differences of Chemical Composition and Optical Properties of Aerosols in the Tibetan Plateau, J. Geophys. Res. Atmos., 125, 10.1029/2019jd031226, 2020.

Xu, J., Hettiyadura, A. P. S., Liu, Y., Zhang, X., Kang, S., and Laskin, A.: Atmospheric Brown Carbon on the Tibetan Plateau: Regional Differences in Chemical Composition and Light Absorption Properties, Environmental Science & Technology Letters, 9, 219-225, 10.1021/acs.estlett.2c00016, 2022a.

Xu, W., Bian, Y., Lin, W., Zhang, Y., Wang, Y., Ma, Z., Zhang, X., Zhang, G., Ye, C., and Xu, X.: O3 and PAN in southern Tibetan Plateau determined by distinct physical and chemical processes, Atmos. Chem. Phys., 23, 7635-7652, 10.5194/acp-23-7635-2023, 2023.

Xu, X., Zhang, H., Lin, W., Wang, Y., Xu, W., and Jia, S.: First simultaneous measurements of peroxyacetyl nitrate (PAN) and ozone at Nam Co in the central Tibetan Plateau: impacts from the PBL evolution and transport processes, Atmos. Chem. Phys., 18, 5199-5217, 10.5194/acp-18-5199-2018, 2018b.

Xu, Y., Li, Q., Xie, S., Zhang, C., Yan, F., Liu, Y., Kang, S., Gao, S., and Li, C.: Composition and sources of heavy metals in aerosol at a remote site of Southeast Tibetan Plateau, China, Science of the Total Environment, 845, 157308, 10.1016/j.scitotenv.2022.157308, 2022b.

Yang, Y., Zhou, R., Yan, Y., Yu, Y., Liu, J., Di, Y., Du, Z., and Wu, D.: Seasonal variations and size distributions of water-soluble ions of atmospheric particulate matter at Shigatse, Tibetan Plateau, Chemosphere, 145, 560-567, 10.1016/j.chemosphere.2015.11.065, 2016.

Yuan, Q., Xu, J., Wang, Y., Zhang, X., Pang, Y., Liu, L., Bi, L., Kang, S., and Li, W.: Mixing State and Fractal Dimension of Soot Particles at a Remote Site in the Southeastern Tibetan Plateau, Environ. Sci. Technol., 53, 8227-8234, 10.1021/acs.est.9b01917, 2019.

Zhang, L., Tang, C., Huang, J., Du, T., Guan, X., Tian, P., Shi, J., Cao, X., Huang, Z., Guo, Q., Zhang, H., Wang, M., Zeng, H., Wang, F., and Dolkar, P.: Unexpected High Absorption of Atmospheric Aerosols Over a Western Tibetan Plateau Site in Summer, J. Geophys. Res. Atmos., 126, 10.1029/2020jd033286, 2021a.

Zhang, N., Cao, J., Liu, S., Zhao, Z., Xu, H., and Xiao, S.: Chemical composition and sources of $PM_{2.5}$ and TSP collected at Qinghai Lake during summertime, Atmos. Res., 138, 213-222, 10.1016/j.atmosres.2013.11.016, 2014.

Zhang, N., Cao, J., Huang, R., He, Y., Wang, Q., and Zhu, C.: Seasonal Variation, Sources and Transport of Aerosols at Lijiang, Southeast Tibetan Plateau, Aerosol Air Qual. Res., 16, 1579-1590, 10.4209/aaqr.2015.07.0470, 2016.

Zhang, Q., Jimenez, J. L., Worsnop, D., and Canagaratna, M.: A case study of urban particle acidity and its influence on secondary organic aerosol, Environ. Sci. Technol., 41, 3213-3219, 10.1021/es061812j, 2007.

Zhang, Q., Jimenez, J. L., Canagaratna, M. R., Ulbrich, I. M., Ng, N. L., Worsnop, D. R., and Sun, Y.: Understanding atmospheric organic aerosols via factor analysis of aerosol mass spectrometry: a review, Anal. Bioanal. Chem., 401, 3045-3067, 10.1007/s00216-011-5355-y, 2011.

Zhang, X., Xu, J., Kang, S., Liu, Y., and Zhang, Q.: Chemical characterization of long-range transport biomass burning emissions to the Himalayas: insights from high-resolution aerosol mass spectrometry, Atmos. Chem. Phys., 18, 4617–4638, 10.5194/acp-18-4617-2018, 2018.

Zhang, X., Xu, J., Kang, S., Zhang, Q., and Sun, J.: Chemical characterization and sources of submicron

aerosols in the northeastern Qinghai–Tibet Plateau: insights from high-resolution mass spectrometry, Atmos. Chem. Phys., 19, 7897-7911, 10.5194/acp-19-7897-2019, 2019.

Zhang, X., Xu, J., and Kang, S.: Chemical characterization of submicron particulate matter (PM_1) emitted by burning highland barley in the northeastern part of the Qinghai–Tibet Plateau, Atmos. Environ., 224, 117351, 10.1016/j.atmosenv.2020.117351, 2020.

Zhang, X., Xu, J., Kang, S., Sun, J., Shi, J., Gong, C., Sun, X., Du, H., Ge, X., and Zhang, Q.: Regional Differences in the Light Absorption Properties of Fine Particulate Matter Over the Tibetan Plateau: Insights From HR-ToF-AMS and Aethalometer Measurements, J. Geophys. Res. Atmos., 126, 10.1029/2021jd035562, 2021b.

Zhang, Y., Xu, J., Shi, J., Xie, C., Ge, X., Wang, J., Kang, S., and Zhang, Q.: Light absorption by water-soluble organic carbon in atmospheric fine particles in the central Tibetan Plateau, Environ. Sci. Pollut. Res., 24, 21386-21397, 10.1007/s11356-017-9688-8, 2017.

Zhao, S., Ming, J., Xiao, C., Sun, W., and Qin, X.: A preliminary study on measurements of black carbon in the atmosphere of northwest Qilian Shan, J. Environ. Sci., 24, 152-159, 10.1016/s1001-0742(11)60739-0, 2012.

Zhao, S., Ming, J., Sun, J., and Xiao, C.: Observation of carbonaceous aerosols during 2006-2009 in Nyainqentanglha Mountains and the implications for glaciers, Environmental science and pollution research international, 20, 5827-5838, 10.1007/s11356-013-1548-6, 2013a.

Zhao, S., Qi, S., Yu, Y., Kang, S., Dong, L., Chen, J., and Yin, D.: Measurement report: Contrasting elevation-dependent light absorption by black and brown carbon: lessons from in situ measurements from the highly polluted Sichuan Basin to the pristine Tibetan Plateau, Atmos. Chem. Phys., 22, 14693-14708, 10.5194/acp-22-14693-2022, 2022a.

Zhao, W., Zhang, X., Zhai, L., Shen, X., and Xu, J.: Chemical characterization and sources of submicron aerosols in Lhasa on the Qinghai–Tibet Plateau: Insights from high-resolution mass spectrometry, Sci. Total Environ., 815, 10.1016/j.scitotenv.2021.152866, 2022b.

Zhao, Z., Cao, J., Shen, Z., Xu, B., Zhu, C., Chen, L.-W. A., Su, X., Liu, S., Han, Y., Wang, G., and Ho, K.: Aerosol particles at a high-altitude site on the Southeast Tibetan Plateau, China: Implications for pollution transport from South Asia, J. Geophys. Res. Atmos., 118, 11360-11375, 10.1002/jgrd.50599, 2013b.

Zhao, Z., Cao, J., Chow, J. C., Watson, J. G., Chen, A. L. W., Wang, X., Wang, Q., Tian, J., Shen, Z., Zhu, C., Liu, S., Tao, J., Ye, Z., Zhang, T., Zhou, J., and Tian, R.: Multi-wavelength light absorption of black and brown carbon at a high-altitude site on the Southeastern margin of the Tibetan Plateau, China, Atmos. Environ., 212, 54-64, 10.1016/j.atmosenv.2019.05.035, 2019a.

Zhao, Z., Wang, Q., Li, L., Han, Y., Ye, Z., Pongpiachan, S., Zhang, Y., Liu, S., Tian, R., and Cao, J.: Characteristics of PM2.5 at a High-Altitude Remote Site in the Southeastern Margin of the Tibetan Plateau in Premonsoon Season, Atmosphere, 10, 645, 10.3390/atmos10110645, 2019b.

Zheng, J., Hu, M., Du, Z., Shang, D., Gong, Z., Qin, Y., Fang, J., Gu, F., Li, M., Peng, J., Li, J., Zhang, Y., Huang, X., He, L., Wu, Y., and Guo, S.: Influence of biomass burning from South Asia at a high-altitude mountain receptor site in China, Atmos. Chem. Phys., 17, 6853-6864, 10.5194/acp-17-6853-2017, 2017.

Zhou, J., Tie, X., Xu, B., Zhao, S., Wang, M., Li, G., Yang, S., Chang, L., and Cao, J.: Black carbon (BC) in North Tibetan Mountain; Effect of Kuwait fires on glacier, Atmospheric Chemistry and Physics Discussions, 1-24, 10.5194/acp-2018-448, 2018.

Zhu, C.-S., Qu, Y., Dai, W.-T., Zhang, N.-N., Zhang, Z.-S., and Cao, J.-J.: Nonnegligible biogenic organic

aerosol and the correlations with light absorption at three high altitude locations in the Qinghai–Tibetan Plateau, Atmos. Environ., 291, 10.1016/j.atmosenv.2022.119394, 2022.

Zhu, C. S., Cao, J. J., Hu, T. F., Shen, Z. X., Tie, X. X., Huang, H., Wang, Q. Y., Huang, R. J., Zhao, Z. Z., Mocnik, G., and Hansen, A. D. A.: Spectral dependence of aerosol light absorption at an urban and a remote site over the Tibetan Plateau, Sci. Total Environ., 590-591, 14-21, 10.1016/j.scitotenv.2017.03.057, 2017.

Zhu, C. S., Cao, J. J., Huang, R. J., Shen, Z. X., Wang, Q. Y., and Zhang, N. N.: Light absorption properties of brown carbon over the southeastern Tibetan Plateau, Sci. Total Environ., 625, 246-251, 10.1016/j.scitotenv.2017.12.183, 2018.

Zhu, C. S., Li, L. J., Huang, H., Dai, W. T., Lei, Y. L., Qu, Y., Huang, R. J., Wang, Q. Y., Shen, Z. X., and Cao, J. J.: n-Alkanes and PAHs in the Southeastern Tibetan Plateau: Characteristics and Correlations With Brown Carbon Light Absorption, J. Geophys. Res. Atmos., 125, 10.1029/2020jd032666, 2020.

Zhu, C. S., Qu, Y., Huang, H., Chen, J., Dai, W. T., Huang, R. J., and Cao, J. J.: Black Carbon and Secondary Brown Carbon, the Dominant Light Absorption and Direct Radiative Forcing Contributors of the Atmospheric Aerosols Over the Tibetan Plateau, Geophys. Res. Lett., 48, 10.1029/2021gl092524, 2021.